Nuclear Instruments and Methods in Physics Research A 348 (1994) 97–104
North-Holland

NUCLEAR
INSTRUMENTS
& METHODS
IN PHYSICS
RESEARCH
Section A

A three layer circular scintillator hodoscope

M. Dahmen, A. Empl, D. Grzonka, K. Kilian, P. Moskal, W. Oelert *, E. Roderburg, K. Röhrich, M. Rook, T. Sefzick, O. Steinkamp, R. Stratmann, J. Thimmel, P. Turek, M. Waters, M. Wolke, M. Ziolkowski

Institut für Kernphysik, Forschungszentrum Jülich – KFA, D-52425 Jülich, Germany

Received 6 April 1994

The rotationally symmetric kinematics of hadronic reactions around the beam direction call for a detector system with an appropriate symmetry. A hodoscope has been invented which optimally meets such conditions. A combination of both contrarotating and straight scintillator elements form a three layer circular hodoscope. The overlap of individual counters defines pixels with a structure reminiscent of a sunflower pattern. Thus, a rather large, granulated and flat detector arrangement has been achieved economically. Such hodoscopes are in operation for measurements at LEAR/CERN and CELSIUS/Uppsala. A third enlarged version is presently being tested and will be used in the Time Of Flight spectrometer (TOF) at COSY/Jülich. The performance of individual detector elements and of the complete system was investigated with various particle beams and cosmic rays. Comparisons with Monte Carlo calculations confirm the operation of the detector.

1. Introduction

Medium energy physics experiments require a 4π acceptance in the center of mass system (cms) for reaction products under investigation. A detector system with rotational symmetry around the beam axis follows naturally the general kinematical conditions. Most favourable and economical would be a segmented design which guarantees the same counting rate for each detector element. To minimize energy- and angle straggling as well as secondary interactions the detector should have low mass. No unnecessary material must be added to the detector volume. For timing and triggering fast detectors are essential. A segmentation allows an on-line multiplicity determination and a check of kinematic correlations. A trigger veto for neutral events should be provided and digitalization of pulse heights should measure the charged particle velocities. Fulfilling all these requirements would provide a rather powerful particle detection instrument.

The basic conceptional idea for such a detector device is a hodoscope which covers the sphere around the target as much as possible. For a fixed target experiment, where the reaction products are boosted towards the forward hemisphere a principal solution is sketched in Fig. 1 consisting of an arrangement of two parts, a forward endcap and a barrel object both subdivided into pixel structures. Obviously this seemingly simple design is able to cope with several of the demands mentioned above. In consideration of the large total surface and timing requirements plastic scintillator is the ideal detector material.

Conflicts occur when aiming for a realization of such an arrangement. A readout of each individual pixel by a photomultiplier would give rise to mechanical problems, light guides would have to be positioned in the detector area adding useless mass and Cherenkov light could contribute uncontrolled signals. Furthermore, the intrinsic dark current of the photomultipliers leads to noise contributions in such a concept, which does not satisfy coincidences between overlapping counters.

A structuring of the total 4π center of mass solid angle area into smaller partitions can be realized by a coinci-

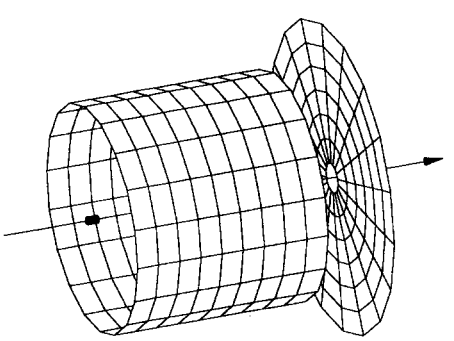

Fig. 1. General and principle concept for a 4π detector in medium energy physics. Target position and beam direction are indicated.

* Corresponding author.

SSDI 0168-9002(94)00512-6

dence disposition of signals from overlapping detector elements, which are arranged in separated scintillator layers.

2. Detector concept

A detector concept becomes reasonably simple and gains essentially in performance when three layers of scintillator elements are combined as shown in Fig. 2 for a forward endcap, where in addition to straight wedge-shaped pieces two layers of twisted scintillator elements are incorporated. These shapes are obtained by bending the straight element around the center by 180°. Thus, the detector introduced here consists of three layers – straight, left and right twisted – combined as shown in Fig. 2 (top) but rather more tightly packed, Fig. 2 (bottom). Each single scintillator element covers the complete polar angle of the detector range which makes this symmetric design especially insensitive to dead time losses.

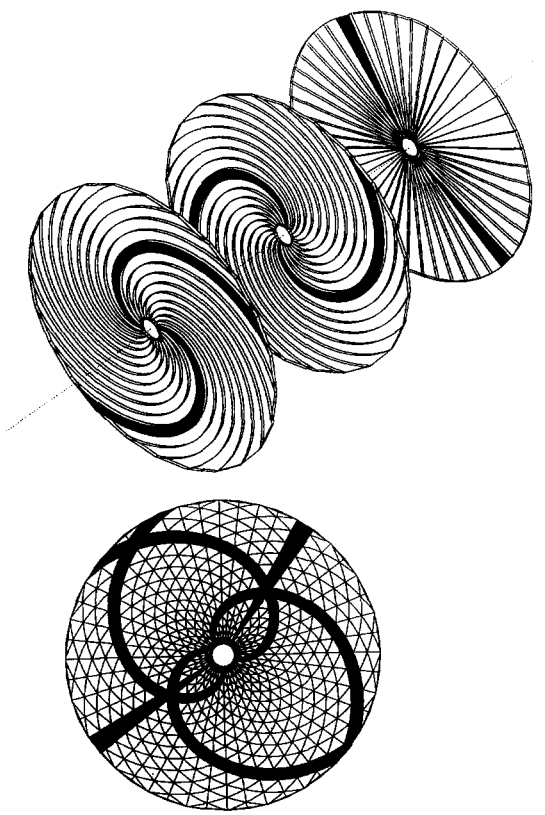

Fig. 2. Top: Exploded view for the three layers of the forward hodoscope. To illustrate the structure the three layers are separated from each other, in the actual experiment the three layers are close to each other. Bottom: Projections of the three layer hodoscope into one plane; two charged particle hits are indicated by darkening of the respective scintillators.

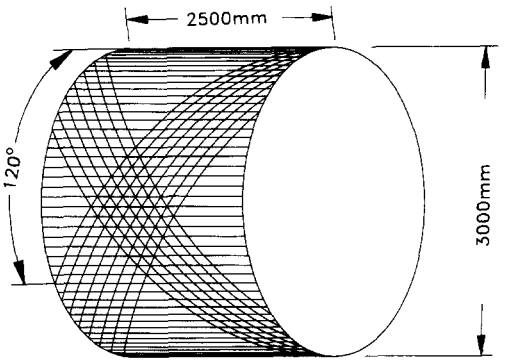

Fig. 3. Sketch of the barrel hodoscope design.

The same construction principle – straight, left and right twisted – is used in the barrel construction as shown in Fig. 3, here for the design of the TOF spectrometer [1]. In this case the bend is only 120° due to feasibility of mounting. By the tight packing of the three layers a highly granulated detector hodoscope with a triangle-like pixel pattern is created.

The elements were produced on a numerically controlled machine from the scintillation material BC404 (Bicron) with 5 mm ± 10% thickness. The active detector is as thin as ≃ 1.5 cm. The outer radius of the active surface for the forward endcap was fixed at 580 mm, whereas the size of the inner hole was adjusted according to each special need, e.g. for an internal beam target experiment it was decided to follow the shape of the beam pipe with a 1 cm space for mounting. The straight scintillator elements – wedges – have a nearly triangular shape as shown in Fig. 4 (left) and since 48 elements are used for the full circle the opening angle is 7.5° for each.

The curves of the twisted scintillators – which we will call "quirls" in the following – are described by Archimedic spirals. In polar coordinates:

$$r(\phi) = (\phi - \phi_i)\frac{R_{\max}}{\phi_{\max}},$$

with $\phi_{\max}$ fixed at 180°, $R_{\max}$ fixed at 580 mm, and $\phi_i - \phi_{i+1} = \Delta\phi = 15°$. Fig. 4 (right) represents the design details of these twisted scintillator detectors. For each of the two layers 24 elements were produced. The readout is performed by photomultipliers (EMI 9954 B) with laminated light guides glued to the scintillator elements.

The light guides were produced out of plexiglas (GS233) with a thickness of 6 mm starting from the outer end of each scintillator element. The light guides for the quirls were continued tangentially to the outer Archimedic curve of the scintillator element. Calculations [2,3] for the direction of the light output – once the light has been produced isotropically inside the quirl scintillator – show that the preferred light path is parallel and with highest probability close to the outside spiral. Following the demand of mini-

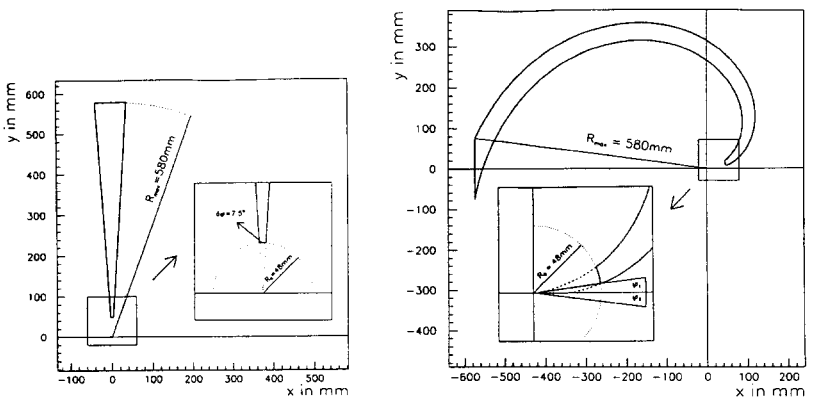

Fig. 4. Details of the wedges (left) and quirls (right) as single elements of the three layer endcap hodoscope.

mal light losses and realistic design requirements a solution has been chosen as presented in Fig. 5 for the top and the side views.

Both at LEAR/CERN and at CELSIUS/Uppsala such systems have been employed in the PS185 [4] and PS202 (JETSET) [5] and in the PROMICE [6] collaborations, respectively. An enlarged system is under construction for the Time Of Flight spectrometer (TOF) [1] at COSY/Jülich.

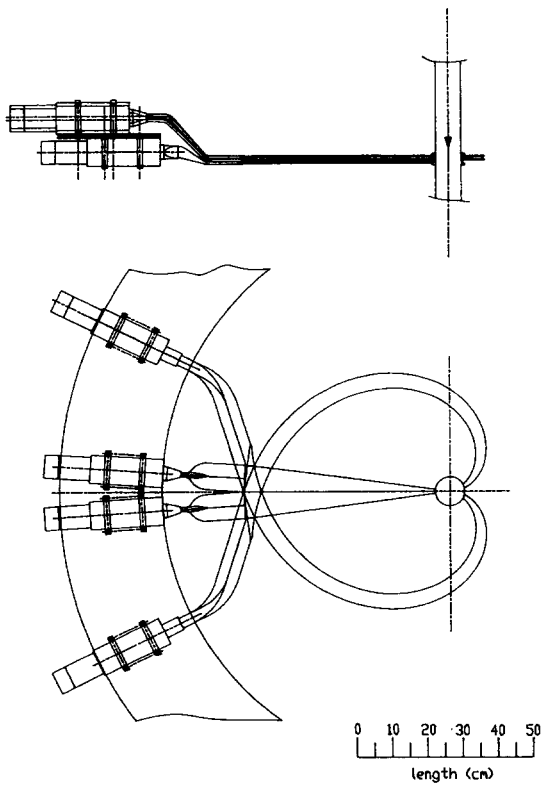

Fig. 5. Side and top view of the arrangement for the hodoscope.

3. Features of the present concept

For the projection of the three layers into one plane (Fig. 2.) two charged particle hits are indicated by dark "active" scintillators. Employing 48 straight wedges and 24 left and right twisted quirls 1152 pixels (diminished by the number of pixels due to the center space occupied by the beam) are formed over an area of $\pi r^2 = 1.06\ \mathrm{m}^2$. Compared to a single element pixel device the suggested detector is much more economic since it needs only 96 photomultiplier channels. The coincidence of two or three scintillation detectors drastically reduces the noise contribution.

A serious disadvantage of a rectangular hodoscope is the unequal coverage of hits from particle reactions. Close to the beam axis the scintillators would see a very high counting rate with decreasing intensity towards their ends. The outer elements of such a hodoscope would count only a fraction of those from the inner part. This disadvantage is omitted in the present design. Each type of the scintillator elements is exposed to the same amount of radiation, where a single wedge element gets half the counting rate of a quirl. The increasing width of each element accounts qualitatively for the unequal distribution of radiation in scattering experiments and makes the scintillator a perfect light guide. It should be mentioned that for each pixel both the radius value Δr as well as the azimuth angle $\Delta\phi$ are constant. The pixel size of a ring (n) around the center is given by:

$$F = \frac{1}{2}\frac{1}{4}\left(\frac{R_{\max}}{\phi_{\max}}\right)^2 (\Delta\phi)^3 n; \qquad n\epsilon\{1,\ldots,23 \text{ and } 24/2\}.$$

In a three layer hodoscope only definite combinations of single elements of the layers are geometrically allowed to give reasonable and valuable information. Numbering the left and right twisted quirls in a free but systematic way the numbers of the fired twisted modules are directly correlated to the hit position. The difference $(i_{\text{left}} - j_{\text{right}})$

is related to the polar angle and the sum $(i_{\text{left}} + j_{\text{right}})$ is proportional to the azimuthal angle. Therefore, due to the highly symmetric structure of the detector a logically simple but logistically sophisticated electronic circuit for a three fold "AND LOGIC" can be used in an on-line trigger condition. Both, cuts on large or small angles and a determination of a fixed angle correlation have been employed in a "pixel trigger" and "luminosity determination via elastic scattering" in ongoing experiments [7,8].

Strongly correlated to the pixel determination is the question of multiplicity. The space between the single elements of each layer is 400 μm, which is needed for light tight wrapping and mounting tolerances. Neglecting this 0.9% of the total area per twisted plane, the multiplicity can be determined directly by counting the number of hits in each layer. Incorrect information would be given in those cases only where two particles of one event pass through the same scintillator element. In most medium energy physics experiments less than eight prong events are typical. Using a three layer hodoscope with a granularity of 48 wedges and 24 quirls the probability "P" of a double hit in one scintillator element is negligible since under these conditions it amounts to $P_{\text{wedge}} = 3.0 \times 10^{-3}$ for a single wedge (4 times as much for a quirl).

It is well known from two layer hodoscopes that two well separated particles will – in addition to the real pixels – feign a second solution with two "ghost" hits, as demonstrated in Fig. 6 for a simple example. A third layer at a different angle would resolve or at least reduce this ambiguity. Still, in cases of larger multiplicities the pixel determination very often results in too high numbers, as shown in Fig. 7 (left). For the case of a statistically produced four prong event [9] the number of pixels counts up to a maximum of eleven whereas the actual correct pixel number has only a probability of 25%.

To minimize these ambiguities [9], a fast three-fold coincidence between a left and right twisted quirl and the equivalent wedge signal should be provided. The comparison of the right part with the left part of Fig. 7 demonstrates the drastic decrease of ambiguities using a 1 ns gate width for the coincidence between the twisted elements

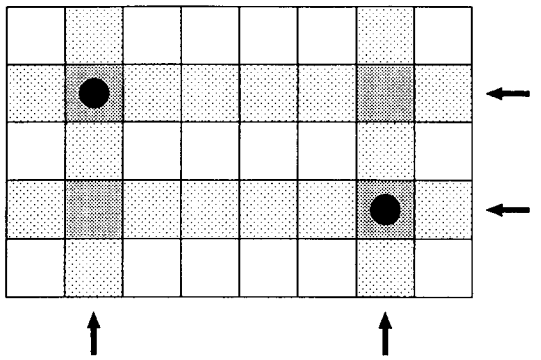

Fig. 6. Two charged particle hits in a two layer rectangular hodoscope; two additional feign hit positions are indicated.

only. Whereas the delay for the two twisted elements is equal, the delay for the wedge has to be pixel dependent.

Off-line reduction of feign pixels is possible under different circumstances as described in Ref. [9].

4. Results

Since especially the twisted elements have a rather nonconventional shape extensive test measurements have been performed using radio-active sources, cosmic rays, a cyclotron beam with 45 MeV protons and the test beam of CERN (T11) with 2 GeV/c protons and pions to study the features of the elements.

Monte Carlo calculations show that the preferential light path is close to the outside curve of the twisted quirl. In order to verify this result experimentally the junction surface of the scintillator to the light guide has been equipped with eleven small light guides followed by photomultipliers (Hamamatsu R1635-2) with a diameter of 3/8 in. Thus, the differential output yield has been measured [2] whereas normally only the integrated yield is recorded. Fig. 8 confirms the calculated results showing that at the outer side ($y = 75$ mm, see Fig. 4 (right)) about 11 electrons were registered on the first dynode decreasing

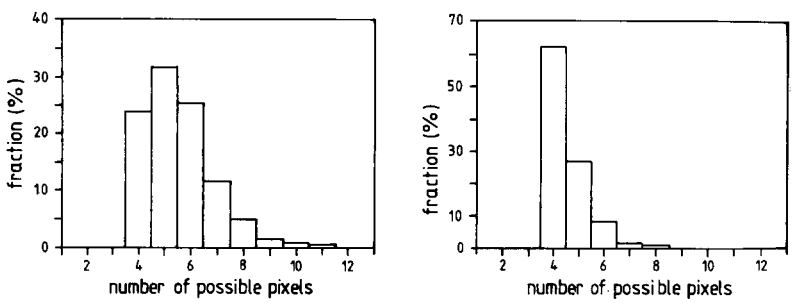

Fig. 7. Number of possible pixels for four charged incident particles, without (left) and with (right) a coincidence (1 ns gate width) between the two twisted scintillators.

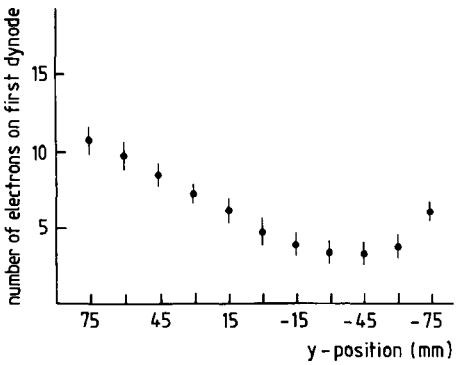

Fig. 8. Number of electrons on the first dynode for an irradiation of the scintillator along the readout surface of the quirl scintillator, see text for discussion and Fig. 4) for dimensions of the Y-axis.

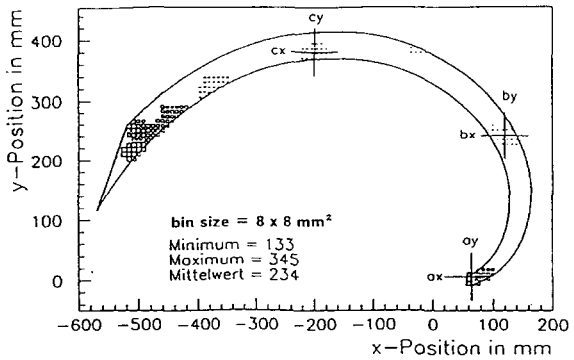

Fig. 10. Light output distribution of a quirl element averaged over bin sizes of 8×8 mm^2. The square of the minimum yield degenerates to a point.

to a minimum value of 2–3 electrons at $y = -40$ mm and followed again by a slight increase towards the inner spiral end at $y = -75$ mm with about 5 electrons. The quirl was irradiated close to its point at the center of the hodoscope. During these measurements the eleven light guides were connected to the scintillator with an angle as used in the final design (Fig. 5); further measurements have been performed with different angles between light guides and scintillator demonstrating the optimum choice selected.

The path length along a spiral of a quirl element is given by:

$$L(\phi) = \frac{r_{\max}}{2\phi_{\max}}\left(\phi\sqrt{1+\phi^2} + \ln\left(\phi + \sqrt{1+\phi^2}\right)\right),$$

thus with the parameters given by the special quirl element for the test measurements ($r_{\max} = 480$ mm, $\phi = 180°$) the path length varies between $L\,(0°) = 0$ mm and $L\,(180°) = 934$ mm. Since the refractive index of the BC404 material used is $n = 1.581$ a velocity of $v_y = 18.96$ cm/ns is expected. Fig. 9 shows the relation of path length versus timing when irradiating the quirl scintillator at different

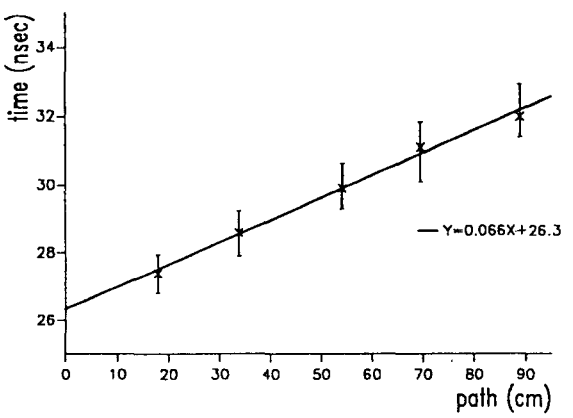

Fig. 9. Relation of time versus path length in a quirl scintillator.

positions of the central spiral. An almost linear dependence is observed. The travelling time is found to be 6.1 ± 0.4 ns which leads to a measured velocity of 15.3 ± 1.2 cm/ns. Due to additional reflections at the scintillator surfaces the effective light path is increased by $24 \pm 8\%$.

Only the well matched timing between all detector elements in the three different layers gives confidence that a true hit has been registered. The need for reduction of ambiguities has been pointed out.

For protons with $\beta = 0.3$, a timing resolution has been observed [10] which varies for different points of irradiation between 0.25 ns and 0.42 ns FWHM. On the other hand, for minimum ionising particles – with only about 10% energy loss as compared to the case of $\beta = 0.3$ – this variation is between 0.6 ns and 1.2 ns FWHM and thus demonstrates the $1/\sqrt{N}$ first order scaling. The spatial light output variation must be understood if the detector – in addition to timing and hit position determination – is to be used for particle identification via energy loss (β-value) measurements.

The quirl element has been exposed [11] to a 2 GeV/c proton and pion beam of CERN (T11) where the hit position was determined by a set of multi-wire chambers and grouped within areas of 8×8 mm^2. Fig. 10 displays the light output distribution of a quirl element. The size of the shown squares is proportional to the relative light output. The minimal output yield (at position $x = 90$ mm and $y = 250$ mm it degenerates to a point) is equivalent to a response of about 50 electrons and the maximum output (at position $x = -520$ mm and $y = 215$ mm it is represented by the largest square) being equivalent to a response of about 130 electrons on the first dynode.

The variations of the light output along the local coordinate systems (ax, ay), (bx, by), and (cx, cy) – as defined in Fig. 10 – were extracted [11] and are shown in Fig. 11. They demonstrate the light output dependence at different places relative to the center spiral. A variation of the signal height between the outer and inner spiral can be

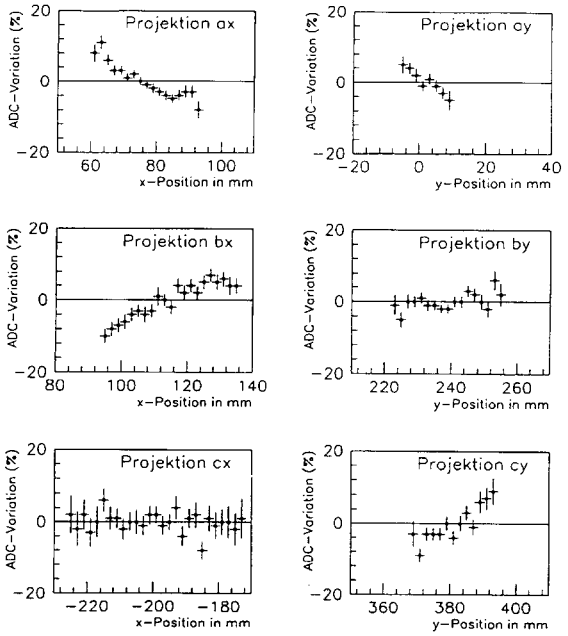

Fig. 11. Selected relative light output as a function of the hit distributions defined in Fig. 10.

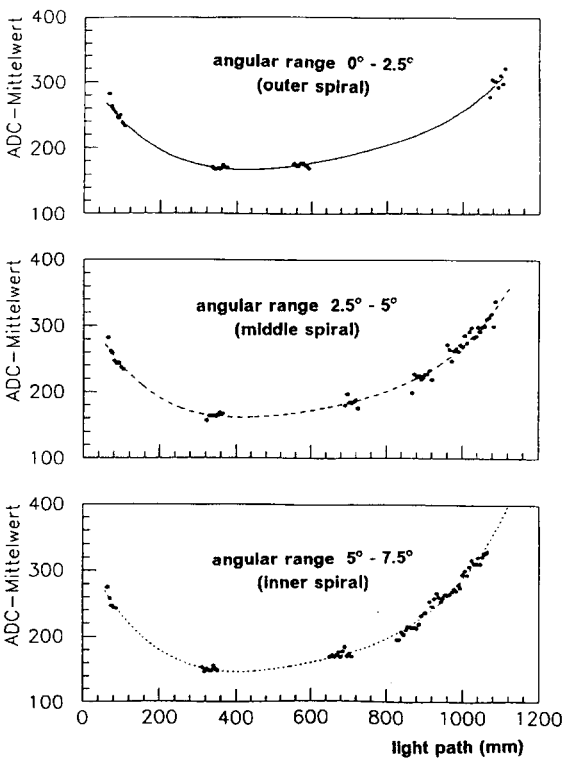

Fig. 12. Output yield of a quirl element along different paths of the Archimedic spiral with its center at 0 mm; top $\phi = 12.5°$, middle $\phi = 7.5°$, bottom $\phi = 2.5°$.

observed. This result shows one of the intrinsic features of the quirl elements which has to be taken into account for energy loss determinations.

Finally, the light output variation along the Archimedic spiral has been determined [11]. The detector element has an opening angle of 15°, a segmentation into three spirals (0°–5°, 5°–10°, 10°–15°) has been defined and the light output along these sub-quirls with centers at 2.5°, 7.5°, and 12.5°, respectively, is shown in Fig. 12. An increase of registered photons towards the two ends of the scintillator (at 0 mm is the center of the hodoscope) is observed. This effect is due the little light attenuation close to the photomultiplier and due to reflections of photons from the tip part of the scintillator which are favoured due to the divergent scintillator shape. The experimental values have been fitted to polynomials of 4th order to get a functional description of the light output:

$$Y(x) = \sum_{i=1}^{4} a_i x^i.$$

The polynomial values can be obtained from Ref. [11] for the quirls as well as for the wedges. For a precise application a calibration of each element is necessary.

The Bethe–Bloch formula describes the energy loss of particles passing through matter which is proportional to the square of the velocity β^2. Therefore, knowing the energy deposit in the scintillator the velocity β can be determined and thus combined with a mass assumption the particle momentum can be calculated. The typical uncertainty of the energy loss measurement within one pixel determined by the yield of the light output is $\sigma = 16\%$ which leads to a particle momentum dependent particle

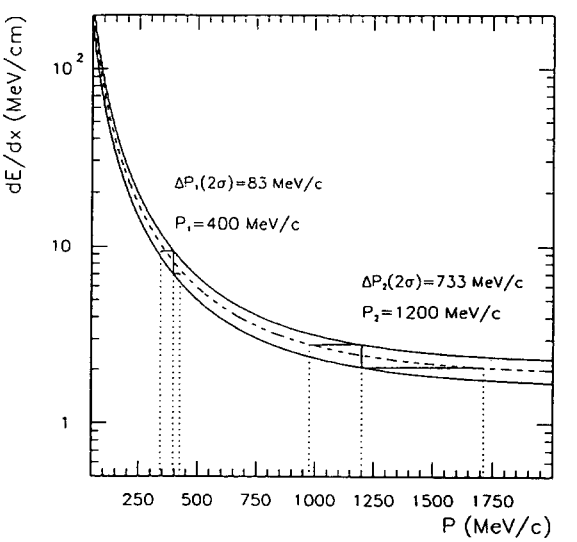

Fig. 13. Bethe–Bloch dE/dx curve for protons (dashed line) with error estimates on the basis of a 16% uncertainty in the measurement of the energy loss value.

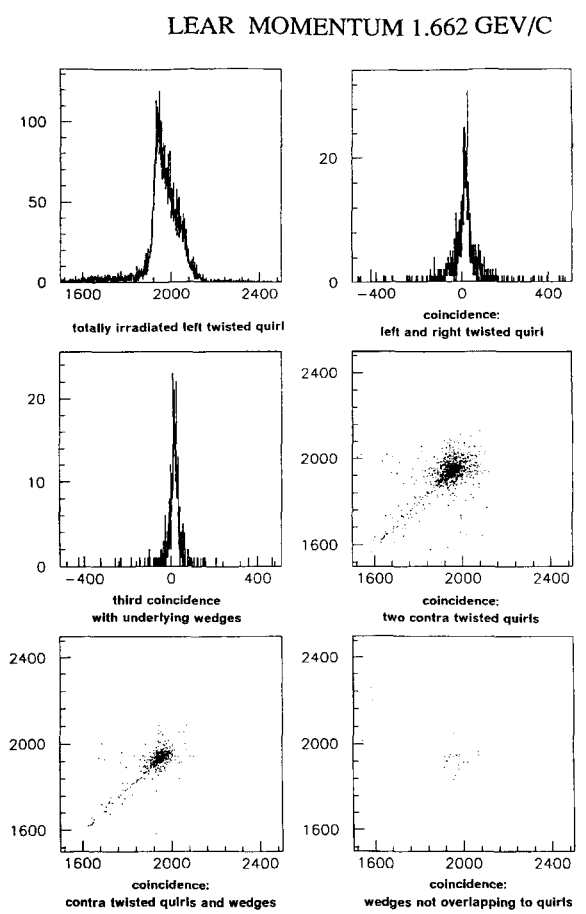

Fig. 14. Selection of TDC spectra of one quirl scintillator element in different coincidence conditions, 50 ps/channel, see text.

momentum uncertainty, as demonstrated in Fig. 13 for the two examples of:

$$P_1 = 400\ \text{MeV}/c(\beta = 0.39) \rightarrow\rightarrow \Delta P = 83\ \text{MeV}/c$$
$$\rightarrow\rightarrow \Delta\beta = -12\% + 5\%,$$
$$P_1 = 1200\ \text{MeV}/c(\beta = 0.79) \rightarrow\rightarrow \Delta P = 733\ \text{MeV}/c$$
$$\rightarrow\rightarrow \Delta\beta = -8\% + 11\%.$$

The TDC spectrum of a totally irradiated left twisted quirl detector in a 1.6 GeV/c antiproton momentum $\bar{p}p$ experiment at LEAR is shown in Fig. 14. The trigger in this experiment was generated by a thin scintillator counter registering each incident beam particle. In the upper left chart of Fig. 14 no coincidence with another detector element was required, resulting in a timing distribution with a width of about 6 ns FWHM due to the shape and size of the quirl element. The time spread reduces drastically when a coincidence between a left and a right twisted segment is required, the difference of the TDC spectra is given in Fig. 14 (top right). However, there are still some hits observed which result in a broadening at the bottom. Demanding a third coincidence of the underlying wedges lowers the background significantly, as seen in Fig. 14 middle left.

The remaining pictures in Fig. 14 show scatter plots. For the two-dimensional TDC spectra of two contra twisted quirls three types of events become apparent in the middle right part of this figure:

(i) The central counts due to particles passing through the detector at the geometrically overlapping region of these two scintillator elements.

(ii) A 45° line indicating an equal timing for the photons to reach the photomultipliers which is due to particles passing through the two quirl elements at the same radius of the detector. Regarding the large time spread of about 45 ns (50 ps/channel), these events are most probably due to accidental coincidences from additional particles hitting the regarded detector pixel within the trigger timing window.

(iii) Two lines horizontal and vertical with few events, where one of the two quirls has been hit in the pixel area, the other seeing an accidental coincidence outside this geometrical pixel range and/or outside the correct timing range but within the trigger time gate.

In the lower left part of Fig. 14 an additional wedge coincidence results in a significant cleaning of the hit pattern. Finally, at the lower right part of Fig. 14 a coincidence is required with a wedge not overlapping geometrically with the quirls. Only 3% of the counts remain compared to the true coincidence case, these few counts obviously are due to multiplicity ≥ 2 events.

5. Summary

The presented quirl detector has been used at LEAR and at CELSIUS very successfully for multiplicity deter-

Table 1

Quantity	Feature
Size	Large: $\simeq 1\ \text{m}^2$
Thickness	Small: $\simeq 1.5$ cm scintillator material for three layers
Material	Small; only active material used in the detector area
Shape	Naturally circular
Orientation	Symmetric around the beam axis
Production	Normal with numerically controlled machines
Light collection	Optimal, due to divergent shapes
Timing	Good: 0.11 ns $\leq \sigma \leq$ 0.55 ns
Multiplicity	Detectable on-line
Spatial resolution	Few cm, depending on granularity and timing resolution
$\theta - \phi$ correlations	Determinable on-line
Velocity determination	Possible but momentum dependent
Losses due to dead-time	Minimal due to design

mination, spatial hit position selection, timing purposes, and dE/dx measurements. The main features are collected in Table 1.

In the PS202 (JETSET) experiment at the internal LEAR beam a barrel scintillator system was also incorporated following topologically the same structure and equivalent features as the forward endcap presently discussed. A scaled-up version is in preparation for experiments at COSY. The first elements for the TOF facility are being tested, further elements are in preparation and in summer 1994 the system will be used for experiments. Additionally, the design of the presented detector device is used on Si- and Ge semiconductor counters [12] for topologically equivalent but obviously geometrically smaller detectors.

Acknowledgements

We would like to thank the Jülich workshop and construction office for their accurate and perfect work, especially H. Hadamek and U. Rindfleisch for their unlimited support.

The help from people at CERN is gratefully acknowledged, we would like to thank especially M. Price, R. Harfield, D. Lacroix, and M. Rebut for their help with numerous details in the construction and production work.

E. Chesi from CERN and D. Mäckelburg from the ZEL at the Forschungszentrum Jülich assisted us in the realization of the trigger device.

The three layer circular scintillator hodoscope has been used at CERN (experiments PS185 and PS202) and at Uppsala (experiment PROMICE); we are indebted to these collaborations for the large amount of efficient work done together.

Last but not least we would like to thank J. Geisbüsch for his very valuable contributions during the first days of designing the detector.

References

[1] P. Turek, for the TOF-Collaboration at Jülich, Proc. Workshop on Meson Production, Interaction and Decay, eds. A. Magiera, W. Oelert, E. Grosse (World Scientific, Singapore 1991) Cracow, Poland, 1991.
[2] A. Empl, Diploma-Thesis, Jül-Spez-510, 1989.
[3] R. Stratmann, Ph. D. Thesis, in preparation, Jülich, Germany, 1994.
[4] R. Tayloe, Ph. D. Thesis, in preparation, University of Illinois, USA.
[5] N. Hamann et al., Proc. Int. School on Physics with Low-Energy Antiprotons, 4th Course: Medium-Energy Antiprotons and the Quark-Gluon Structure of Hadrons, Erice, 1990, eds. R. Landua, J.M. Richard and R. Klapisch (Plenum, New York, 1990).
[6] U. Schubert, for the Promice-Collaboration at Uppsala Workshop of International Conference on Meson – Nucleus Interactions Cracow, Poland, 1993, to be published.
[7] K. Röhrich and P. Harris, Annual Report 1992, IKP - KFA Jülich, Jül-2726; J. Majewski, A. Misiak, W. Oelert, T. Sefzick, and M. Ziolkowski, Annual Report 1991, IKP - KFA Jülich, Jül-2590.
[8] K. Kilian, W. Oelert, K. Röhrich, M. Rook and O. Steinkamp, Annual Report 1992, IKP - KFA Jülich, Jül-2726.
[9] T. Sefzick, Diploma Thesis, Jül-Spez-480, 1988.
[10] A. Empl, K. Kilian, W. Oelert, T. Sefzick, and R. Thomas; Annual Report 1989, IKP - KFA Jülich, Jül-Spez-562.
[11] J. Thimmel, Diploma Thesis, Jül-2804, 1993.
[12] H. Machner, for the GEM-Collaboration, Proc. Workshop on Meson Production, Interaction and Decay 1991, Cracow, Poland, eds. A. Magiera, W. Oelert and E. Grosse (World Scientific, Singapore, 1991).